Polymer 99 (2016) 273–280

Contents lists available at ScienceDirect

Polymer

journal homepage: www.elsevier.com/locate/polymer

Effects of polydispersity, additives, impurities and surfaces on the crystallization of poly(ethylene oxide)(PEO) confined to nanoporous alumina

Yasuhito Suzuki [a], Martin Steinhart [b], Michael Kappl [a], Hans-Jürgen Butt [a], George Floudas [c, *]

[a] Max Planck Institute for Polymer Research, 55128, Mainz, Germany
[b] Institut für Chemie neuer Materialien, Universität Osnabrück, D-49069, Osnabrück, Germany
[c] Department of Physics, University of Ioannina, 45110, Ioannina, Greece

ARTICLE INFO

Article history:
Received 4 February 2016
Received in revised form
22 June 2016
Accepted 6 July 2016
Available online 12 July 2016

Keywords:
Heterogeneous/homogeneous nucleation
Confinement
Poly(ethylene oxide)

ABSTRACT

The effects of polydispersity, additives, impurities, free top layer and of surface roughness on the nucleation are studied for poly(ethylene oxide) located inside self-ordered nanoporous aluminum oxide (AAO). AAO pore diameters ranged from 400 nm to 25 nm. With the exception of a surface layer, none of the above factors is able to induce heterogeneous nucleation under confinement. Homogeneous nucleation remains the sole mechanism in pores having diameters below 65 nm. The internal pore surface roughness is small, which explains the minor effects of AAO surfaces on inducing heterogeneous nucleation especially within the smaller pores. The presence of oligomers shifts the homogeneous nucleation temperature to lower temperatures, reflecting the plasticizing effect of the oligomers on the liquid-to-glass temperature.

1. Introduction

Polymers crystallize via *heterogeneous* or *homogeneous* nucleation, respectively, at low and high supercooling. In bulk polymers homogeneous nucleation is a rare event. It reflects an intrinsic property that involves crossing a characteristic nucleation barrier. In the majority of cases polymers will crystallize by crossing a significantly lower energy barrier by a mechanism extrinsic to the polymer, known as heterogeneous nucleation [1–3]. Heterogeneous nucleation can in principle be initiated by different sources, *i.e.,* by external nucleating agents (for example, sorbitol-based agents in polyethylene and calcium suberate or sodium benzoate selective to the β-form crystals in isotactic polypropylene (iPP)), by additives (such as remaining catalyst, remaining solvent, other chemicals, and perhaps chain polydispersity), external surfaces (like dust or bubbles), and rough container surfaces.

Despite recent work, very little is known on the precise origin of heterogeneities in polymers giving rise to heterogeneous nucleation [4–17]. For example, it is well-known that crystallizable polymers form superstructures, called spherulites. Yet it is unknown why spherulitic size varies strongly from system to system. Since each spherulite is initiated from a heterogeneity in its center, the number of spherulites is proportional to the number of defects or impurities that catalyze the nucleation. In the case of iPP [4] and poly(ε-caprolactone) (PCL) [5,6], spherulites upon impingement have average sizes in the range from 10 to 50 μm indicating a high density of heterogeneous nuclei. However, in the case of poly(ethylene oxide) (PEO) [7], spherulites have on average a diameter of ~300 μm, and in some cases they can reach mm sizes and can be observed by naked eye. This suggests that PEO is relatively free from impurities and as such it has a higher propensity to crystallize via homogeneous nucleation under confinement.

In the bulk, a single nucleus can in principle crystallize (heterogeneously) the whole sample. Recent studies of polymer crystallization within nanometer size pores demonstrated that by confining polymers to small isolated volumes one can nearly completely suppress heterogeneous nucleation in favor of homogeneous nucleation [4–7]. In this respect, PEO is a model system as it best shows the transformation from heterogeneous to homogeneous nucleation upon confinement [6,7]. Indeed, confining PEO within self-ordered nanoporous aluminum oxide (anodic

* Corresponding author.
E-mail address: gfloudas@uoi.gr (G. Floudas).

http://dx.doi.org/10.1016/j.polymer.2016.07.021
0032-3861/

aluminum oxide, abbreviated as AAO) revealed that heterogeneous nucleation is completely suppressed within pores with diameters below 65 nm. In a simple view, this finding may imply that heterogeneities are impurities extrinsic to the polymer; inserting polymer chains to isolated nanometer size volumes effectively excludes these "impurities".

Hence, the main crystallization mechanism upon confinement is through homogeneous nucleation. This size exclusion mechanism potentially opens a new way of understanding the origin of heterogeneous nucleation. These ideas were recently expanded to ice formation within the same AAO templates [18–20]. In all these studies, AAO templates play a crucial role. AAO contain arrays of discrete-isolated, parallel, cylindrical nanopores that are uniform in length and diameter [21–24]. Of particular importance here is the role of the AAO surface in the nucleation mechanism. Despite recent work, there are still issues related to heterogeneous nucleation that remain unanswered. A significant advantage in the field has been provided via fast scanning chip calorimetry that resolved the processes of heterogeneous and homogeneous nucleation at low and high supercooling, respectively. The distinction was also made based on the higher nucleation density for homogeneous nucleation [25–27].

With the aim to better understand the origin of heterogeneous nucleation, herein we investigate the effects of (a) additives (oligomeric and polymeric), (b) chain polydispersity, (c) blending, (d) a surface layer and (e) the pore surface roughness on the nucleation of polymers confined within AAO templates. These issues provide stringent tests to the nucleation process that can differentiate between *intrinsic* and *extrinsic i.e.,* impurity or surface related effects. For obvious reasons (low nucleation density) the system of choice is PEO. We found that with the exception of a surface layer, none of the above factors is able to induce heterogeneous nucleation under confinement. In addition, by employing EO oligomers as a diluent to PEO we test the hypothesis that the homogeneous nucleation temperature is linked to the liquid-to-glass temperature. Our results show that one can control the homogeneous nucleation temperature by exerting control over the liquid-to-glass temperature (T_g).

2. Experimental

2.1. Samples and methods of infiltration

Poly(ethylene oxide) (PEO) samples with number-averaged molecular weights of 2005 g/mol were synthesized by J. Thiel and T. Wagner (MPI-P) by anionic polymerization. Poly(ε-caprolactone) (PCL) sample with a number-averaged molecular weight of 7700 g/mol was obtained from Polymer Source Inc. and used as received. The notation used here is EO_x and CL_y, where x,y are PEO and PCL degrees of polymerization, respectively. Self-ordered nanoporous aluminum oxide (AAO) (pore diameters of 25, 35, 65, 200 and 400 nm; pore depth 100 μm) was prepared following the procedures reported in the literature [21–23]. Infiltration of samples was performed from chloroform solutions. Typically, 100 mg of bulk PEO and the corresponding additives were dissolved in 10 ml of chloroform. Subsequently, the solution was dropped as a single drop on the top of AAO for a period of 1 h. Lastly, the polymer infiltrated AAOs were placed in a vacuum oven (200 mbar) at 373 K for 1 h. Solution deposition and solvent evaporation were repeated 3 times until reaching a constant polymer mass: 400 nm (~5 mg), 200 nm (~2 mg), 65 nm (~3 mg), 35 nm (~3 mg) and 25 nm (~3 mg). Prior to DSC, excess amount of polymer was removed from the surface of the self-ordered AAO membranes with razor blades and soft polishing paper (Buehler Microcloth). In one case, *i.e.,* when examining the effect of a polymer surface layer on the nucleation process, a thin polymer layer was left intentionally at the top surface.

2.2. Differential scanning calorimetry (DSC)

Thermal analysis was carried out using a Mettler Toledo differential scanning calorimeter (DSC-822). DSC traces of neat PEO were acquired using an empty pan as reference. The sample mass in the infiltrated AAO was estimated from the mass difference between PEO infiltrated AAO and empty AAO. Samples were weighed with a Mettler Toledo AX205 balance. Prior to any DSC measurement, the Al substrates to which the AAO layers had been connected were etched with solutions containing 1.7 mg $CuCl_2 \cdot 2H_2O$, 50 ml deionized H_2O and 50 ml concentrated $HCl_{(aq)}$ under cooling with ice water. Subsequently, the samples were further milled to powder, and 3.0–5.5 mg sample material was sealed in aluminum pans (100 μl). The size of the powder did not affect the nucleation mechanism. DSC traces of infiltrated self-ordered AAO were recorded using reference pans containing empty AAO pieces of the same pore diameter. All samples were first cooled at a rate of 10 °C/min from ambient temperature to −100 °C and then heated to 120 °C at the same rate under a nitrogen atmosphere. The same cycle was repeated two times. Melting and crystallization points, as well as heats of fusion and of crystallization were determined from the second heating and cooling thermograms, respectively.

2.3. Scanning electron microscopy (SEM)

Scanning electron microscopy (SEM) images were obtained using a LEO Gemini 1530 SEM with acceleration voltages from 0.75 to 6 kV Fig. 1 shows top images of AAOs infiltrated with pure PEO and with mixtures of PEO with an oligomer (EO_{46}/EO_3 (90/10)).

2.4. Atomic force microscopy (AFM)

Exposed inner surfaces of the pore walls were imaged using a JPK Nanowizard III (JPK Instruments, Berlin) atomic force microscope in intermittent contact mode, using an AFM cantilever with a nominal tip radius of 5–10 nm, a nominal spring constant of 42 N/m and a resonance frequency of 352 kHz (OMCL-AC160TS, Olympus, Tokyo). The AFM tip was located above the AAO region of the sample using the top view video optics of the AFM. In this procedure the sample was aligned manually to have the pore axis perpendicular to the scan direction of the AFM tip. To determine the root-mean-square (RMS) roughness of the pore walls, the image data were processed with the JPK Data Processing software (Version 5.1.7, JPK Instruments).

2.5. Dielectric spectroscopy (DS)

Dielectric measurements were performed under "isothermal" conditions using a Novocontrol Alpha frequency analyzer (frequency range from 10^{-2}–10^6 Hz). For the infiltrated self-ordered AAO samples, a 10 mm electrode was placed on top of the templates whereas the Al in the bottom of the templates served as the second electrode. The measured dielectric spectra were corrected for the geometry [28] by using two capacitors in parallel (composed of ε^*_{PEO} and ε^*_{AAO}, being the complex dielectric function of PEO and alumina, respectively). The measured total impedance was related to the individual values through $1/Z^* = 1/Z^*_{PEO} + 1/Z^*_{AAO}$. This equation allows calculating the real and imaginary parts of the dielectric permittivity as a function of the respective volume fractions by using: $\varepsilon^*_M = \varepsilon^*_{PEO}\phi_{PEO} + \varepsilon^*_{AAO}\phi_{AAO}$. The complex dielectric permittivity $\varepsilon^* = \varepsilon' - i\varepsilon''$, where ε' is the real and ε'' is the imaginary part, is a function of frequency ω, temperature T, and pressure P

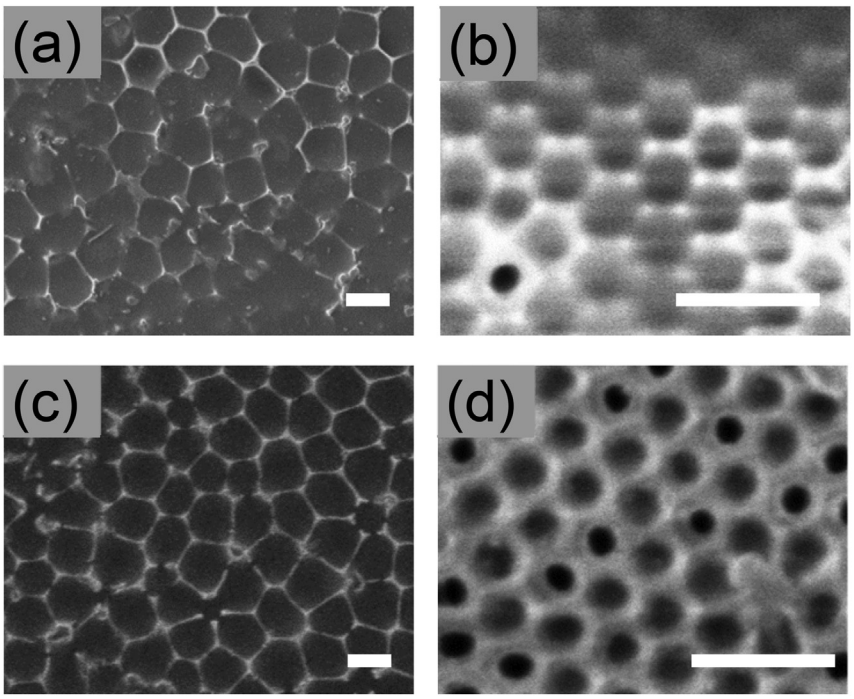

Fig. 1. Scanning electron microscopy images of PEO (a, b) and mixture of PEO/oligomer (c, d) infiltrated in AAO with a pore diameter of 400 nm (a, c) and 65 nm (b, d) from the top. The scale bars indicate 500 μm.

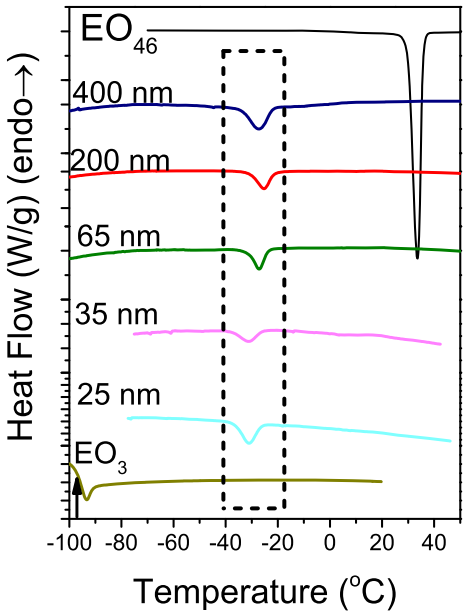

Fig. 2. Thermograms of bulk EO_{46}, pure oligomer (EO_3) and of EO_{46}/EO_3 (90/10) mixture located inside self-ordered AAO with different pore diameters as indicated. All thermograms are obtained on cooling with a rate of 10 K/min. The dashed rectangle indicates the temperature range of homogeneous nucleation. The vertical arrow indicates the glass temperature of the oligomer.

$\varepsilon^* = \varepsilon^*(\omega, T, P)$ [29–31]. In the analysis of the DS spectra we have used the empirical equation of Havriliak and Negami (HN) [32]:

$$\varepsilon^*_{HN}(\omega, T) = \varepsilon_\infty(T) + \frac{\Delta\varepsilon(T)}{\left[1 + (i\omega \cdot \tau_{HN}(T))^m\right]^n} + \frac{\sigma_0(T)}{i\varepsilon_f\omega} \quad (1)$$

where $\tau_{HN}(T,P)$ is the characteristic relaxation time, $\Delta\varepsilon(T,P) = \varepsilon_0(T,P)$-$\varepsilon_\infty(T,P)$ is the relaxation strength of the process under investigation, m, n (with limits $0 < m$, $mn \leq 1$) describe, respectively, the symmetrical and unsymmetrical broadening of the distribution of relaxation times, σ_0 is the dc-conductivity and ε_f is the permittivity of the free space. In the fitting procedure, we have used the ε'' values at every temperature and in some cases the ε' data were also used as a consistency check. From, τ_{HN} the relaxation time at maximum loss, τ_{max}, is obtained analytically following:

$$\tau_{max} = \tau_{HN} \cdot \sin^{-1/m}\left(\frac{\pi m}{2(1+n)}\right) \cdot \sin^{1/m}\left(\frac{\pi mn}{2(1+n)}\right) \quad (2)$$

3. Results and discussion

3.1. Effect of oligomers

Earlier work on the crystallization of PEO as a function of molecular weight indicated some correlation between the homogeneous nucleation temperature and the liquid-to-glass temperature, T_g [7]. This correlation was based on the dependence of the temperature of homogeneous nucleation versus the molecular weight of the polymer, $T_c(M_w)$ which followed $T_c = T_c^\infty$-A/M_w, where A is a constant and T_c^∞ is the temperature of homogenous nucleation in the limit of very high molecular weight within the pores. This dependence is similar to the Fox-Flory equation for $T_g(M_w)$. The hypothesis can be tested by preparing mixtures of PEO with its oligomer. If the liquid-to-glass (T_g) and homogeneous nucleation temperatures (T_c) are related, a shift of the former should produce a concomitant shift in the latter. It is well-known that oligomers impart mobility and as a result lower the liquid-to-glass temperature by a process known as external plasticization. In fact, a polymer/solvent mixture is expected to show two glass temperatures: one corresponding to the plasticized polymer segmental dynamics

and another corresponding to the plasticizer itself [33,34]. This has been demonstrated in several polymer/diluent studies and even in mixtures composed of the same chemistry (*e.g.,* polystyrene/oligostyrene). The latter are fully miscible and possess large dynamic asymmetry (*i.e.,* large difference in their bulk glass temperatures) yet show dynamic heterogeneity with two distinct glass temperatures [33]. Our interest here is mainly on the polymer segmental dynamics. Therefore we concentrate on the "high" plasticized polymer glass temperature.

Fig. 3 depicts cooling thermograms of bulk EO_{46}, of pure oligomer (EO_3) and of EO_{46}/EO_3 (90/10) mixtures located inside AAOs with different pore diameters. As expected, bulk PEO crystallizes via heterogeneous nucleation at ~33 °C (rate −10 °C/min) and predominantly via homogeneous nucleation in the smaller pores. On the other hand, the oligomer shows only a liquid-to-glass temperature at −96 °C. Fig. 3a depicts thermograms of EO_{46} and of EO_{46}/EO_3 mixtures (10 wt% of oligomer (EO_3)) located inside 35 nm AAO pores. On average, a 5 °C shift of homogeneous nucleation temperature due to the addition of oligomer was observed (Fig. 3b). The experiment reveals that it is possible to control the homogeneous nucleation temperature by adding small amounts of diluent.

Dielectric spectroscopy (DS) was employed to follow the segmental dynamics of EO_{46} and of EO_{46}/EO_3 (90/10) mixtures located inside the AAO templates. When PEO is located within AAO templates, PEO segments in the amorphous domains are confined by crystalline domains and by the templates. Relaxation times of the segmental (α-) process at maximum loss in the absence and presence of oligomer (EO_3) are plotted in Fig. 4. Both are fitted with the Vogel-Fulcher-Tammann (VFT) equation:

$$\tau = \tau_0 \exp(B/T - T_0) \quad (3)$$

where τ_0 ($=10^{-12}$s) is the relaxation time in the limit of very high temperatures, B is the activation parameter and T_0 the "ideal" glass temperature. The α-process becomes faster in the presence of oligomer and hence the liquid-to-glass temperature shifts to lower temperatures. The liquid-to-glass temperature of confined EO_{46} (−61 °C) is reduced in the presence of oligomer to −67 °C. This temperature change is in good agreement with the shift of homogeneous nucleation temperature due to the addition of EO_3. The result supports the proposed correlation between homogeneous nucleation temperature and liquid-to-glass temperature.

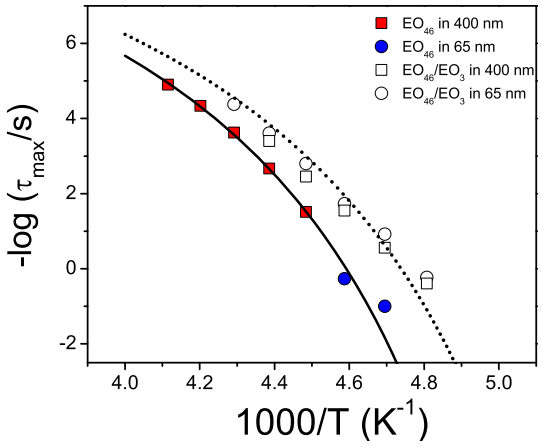

Fig. 4. Relaxation times of the α-process at maximum loss corresponding to PEO_{46} in the absence (filled symbols) and presence (empty symbols) of the oligomer EO_3 located inside AAO pores with pore diameters of 400 nm (squares) and 65 nm (circles). Solid and dashed lines are fits to the corresponding segmental processes with the Vogel-Fulcher-Tammann (VFT) equation (see text).

Given the proximity of the homogeneous nucleation temperature to the liquid-to-glass temperature an open question is how the spatio-temporal heterogeneities associated with the latter temperature relate to the mechanism of homogeneous nucleation [35]. This point deserves further studies by probing both the spatio-temporal heterogeneities (*e.g.,* by single molecule spectroscopy) and its relation to homogeneous nucleation.

An additional comment here is on the possible enrichment of pores during the filling process by the oligomers because of kinetic (higher mobility) and thermodynamic reasons (conformational entropy). This scenario though can be excluded by the single ("plasticized") glass temperature as well as by the single homogeneous nucleation temperature.

3.2. *Effect of chain polydispersity*

The question is, weather very polydisperse polymers, composed of entangled and unentangled chains, could influence the

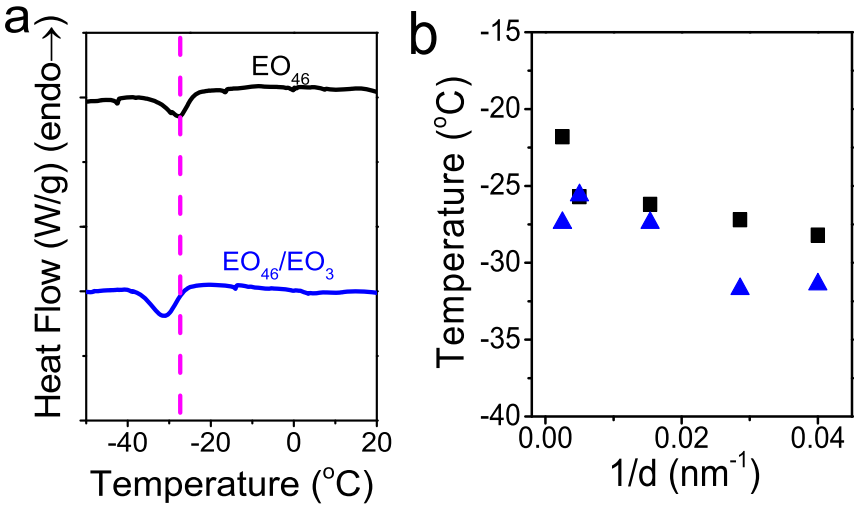

Fig. 3. (a) Comparison of thermograms of EO_{46} located inside AAO in the absence and presence of oligomer (EO_3) with a pore diameter of 35 nm. The cooling speed was 10 °C/min. (b) Homogeneous nucleation temperatures of pure EO_{46} (black squares) and EO_{46} in the presence of oligomer (blue triangles) located inside AAO as a function of inverse pore diameter. On average, a shift of 5 °C in the respective homogeneous nucleation temperatures is observed. (For interpretation of the references to colour in this figure legend, the reader is referred to the web version of this article.)

nucleation process through the very different dynamics and different entanglement density, for example, by inducing heterogeneous nucleation. This effect is different from the addition of oligomer as the polymer there was unentangled (M_e(PEO)~1700 g/mol) [36]. As we discussed earlier, the homogeneous nucleation temperature has pronounced molecular weight dependence [7]. The lower the molecular weight, the lower the homogeneous nucleation temperature is. For relatively high molecular weights, the homogeneous nucleation temperature saturates at ~ -6 °C. In this experiment, 10 wt% of high molecular weight, well-entangled PEO (EO_{2270}), was mixed with a nearly unentangled PEO (EO_{46}), employed also in the first case. Fig. 5a depicts the DSC traces of bulk EO_{2270} and of EO_{2270} infiltrated within AAO with different pore sizes. As with the lower molecular weight sample, EO_{2270} shows a dominant homogeneous nucleation mechanism in confinement. Furthermore, the higher temperature of homogeneous nucleation in EO_{2270} (−20 °C) as compared to EO_{46} (−30 °C) reflects the higher molecular weight. Fig. 5b, gives the thermograms of EO_{46}/EO_{2270} (90/10) mixtures located inside AAO. Since the homogeneous nucleation temperature of EO_{46} is lower than that of EO_{2270}, addition of EO_{2270} could increase the homogeneous nucleation temperature. The DSC traces (Fig. 5b) however, depict a single nucleation event at the low temperature (~-30 °C) corresponding to the majority polymer, *i.e.,* to the unentangled EO_{46}.

A single nucleation process can have two possible origins: (i) EO_{46} may suppress the homogeneous nucleation of EO_{2270} and/or (ii) the homogeneous nucleation temperature of EO_{2270} is shifted to lower temperature and coincides with the homogeneous nucleation temperature of PEO_{46} because of the faster segmental dynamics. In this view, the segmental dynamics of EO_{2270} are plasticized by the shorter chains of EO_{46}. Mixing with a highly entangled polymer *does not* induce heterogeneous nucleation sites. It suggests that polydispersity and entanglement density does not promote heterogeneous nucleation.

3.3. Effect of blending

Melt miscible blends are dynamically and, to a lesser extent, structurally heterogeneous. This type of heterogeneity might enhance the propensity for heterogeneous nucleation. To test this hypothesis we blended 5 wt% of poly(ε-caprolactone) (CL_{68}) with 95 wt% of EO_{46}. PCL is a semicrystalline polymer whose crystallization behavior under the uniform confinement of AAOs was recently investigated [5,6]. PEO and PCL are miscible in the melt state [6,37]. Because of the high nucleation density in the melt, it exhibits both heterogeneous and homogeneous nucleation under confinement in the larger and smaller pores, respectively. Should PCL act as heterogeneous nucleation agent, then the dominance of heterogeneous nucleation is to be expected in its blends with PEO as well. As can be seen in Fig. 6, in the asymmetric (95/5) blend EO_{46}/CL_{68}, homogeneous nucleation remains the main nucleation mechanism under confinement. Furthermore, the homogeneous nucleation temperatures nicely match to those of EO_{46} inside the same AAO pores. Both, the effects of blending and polydispersity considered together, they further support the notion that heterogeneities responsible for nucleation are extrinsic to the polymer.

3.4. Effect of top polymer layer on the AAO surface

It is known that a bulk reservoir on the top of AAO templates can drastically change the nucleation mechanism [24]. In this case all pores "communicate" through the reservoir and a single nucleation event eventually triggers crystallization within all pores. This experiment is expected to enhance heterogeneous nucleation at the expense of homogeneous nucleation. In addition, strong orientation effects of the lamellar crystals are to be expected, as in this case, only certain lamellae orientations can grow [38]. As an example, non-isothermally crystallized poly(vinylidene difluoride) (PVDF) from a bulk reservoir within the same pores shows alignment of the crystallographic direction with the highest growth rate (<020>) with the pore axis [38]. Here the effect of a top layer on PEO crystallization was investigated. In this case intentionally, the surface of AAO was not perfectly cleaned leaving a layer of PEO on top of the template. We chose PEO because of the large spherulites in bulk PEO and the small number of heterogeneous nuclei, a stronger effect is expected with a shift from homogeneous to

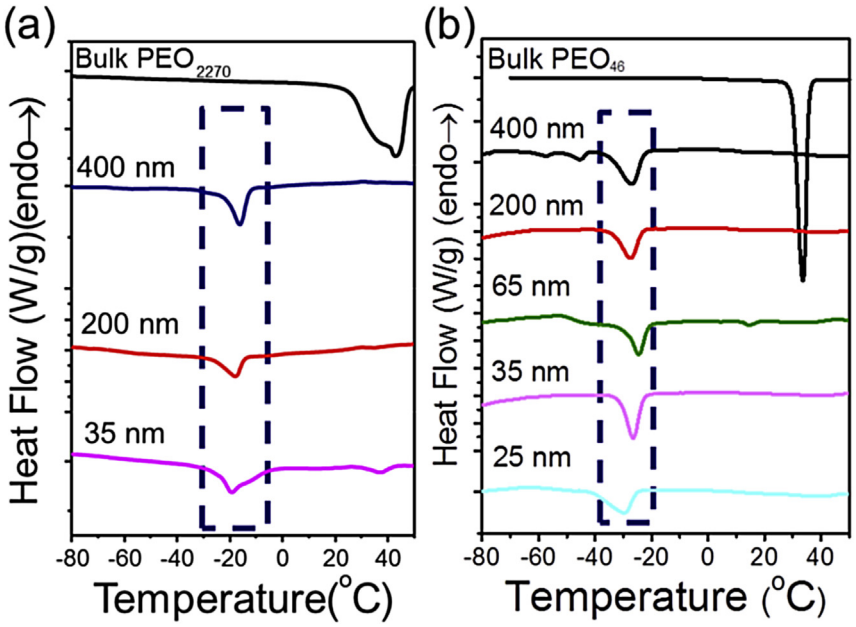

Fig. 5. (a) Thermograms of bulk PEO_{2270} (black line) and of PEO_{2270} located inside AAO with different pore sizes as indicated. The dashed rectangle indicates the temperature range of homogeneous nucleation. (b) Thermograms of bulk PEO_{46} and of EO_{46}/EO_{2270} (90/10) mixtures located inside AAO. The dashed rectangle indicates the temperature range of homogeneous nucleation. All traces refer to cooling runs with the same rate (10 °C/min).

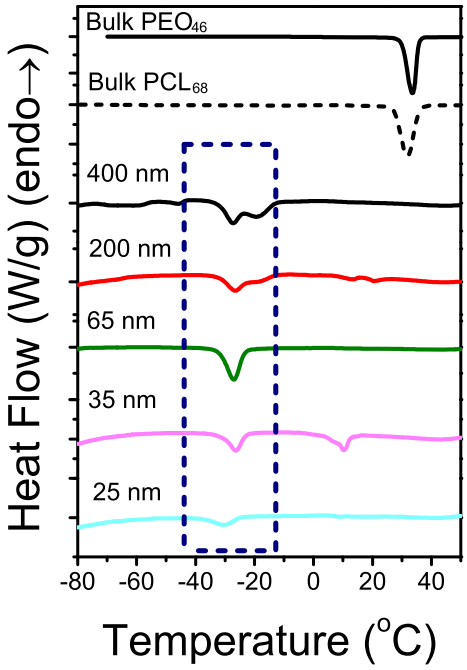

Fig. 6. Thermograms of bulk PEO_{46} (black solid line), bulk PCL_{68} (black dashed line) and of a mixture of EO_{46}/CL_{68} (95/5) located inside AAOs with different pore sizes as indicated. All traces refer to cooling rates of 10 °C/min. The dashed rectangle indicates the temperature range of homogeneous nucleation.

heterogeneous nucleation.

Prior to the DSC experiment, the template with a top layer of EO_{46} was investigated with AFM. Typically, the film thickness was around 500 nm. As an example, an AFM phase image on top of AAO is shown in Fig. 7b. Spiral PEO structures due to self-assembly in a thin film are observed. Fig. 7a depicts DSC traces of bulk EO_{46} and of EO_{46} located inside AAO with different pore diameters in the presence of the surface layer. Measurements were made on heating and subsequent cooling with a rate of 10 °C/min. The DSC traces are now fundamentally different from PEO that crystallized within AAOs but in the absence of a top layer (with respect to Fig. 2). In the presence of top layer, crystallization via heterogeneous nucleation becomes the dominant nucleation mechanism even in the smaller pores (65 nm and 35 nm). In addition, at least two heterogeneous nucleation peaks were observed from EO_{46} confined to AAO with diameters below 200 nm. The stronger peak is slightly shifted to lower temperatures compared to the bulk heterogeneous nucleation temperature. The weaker peak is intermediate to the main heterogeneous and homogeneous nucleation temperature and depends on pore diameter. A plausible explanation is as follows; spherulites impinge on the pore mouths and offer external surfaces for heterogeneous nucleation of the material in the pores. If the thus-formed crystals have their main growth direction not aligned with the pore axes, they will impinge on the pore walls. However, these crystals offer in turn surfaces for further heterogeneous nucleation events until a crystal is oriented in such a way that it can grow straight down the pore. Alternatively, different heterogeneities with variable activities may also nucleate at different temperatures. In theory, crystallization in bulk can be nucleated by heterogeneity of one kind, whereas in the pores, another type of heterogeneity can be activated.

Although, at present, we are unable to fully explain the origin of the intermediate peak, it is evident that the nucleation processes are biased towards heterogeneous nucleation in the presence of a top layer. Furthermore, upon confinement a clear broadening of melting peak is observed. This implies a broader distribution of lamellar thicknesses.

3.5. Roughness of internal pore surface

Rough container surfaces can in principle act as nucleation centers for heterogeneous or surface nucleation. Within a single AAO nanopore, the probability for wall-induced nucleation scales with the surface area; it is reduced by 3 times in going from 65 nm to 25 nm pores and by 16 times in going from 400 nm to 25 nm pores. Hence the expectation that surface-induced nucleation should be significant in larger pores and less significant in smaller pores. In accord with this expectation, earlier studies on PEO located inside 400 nm pores [7] and of PCL located inside 400 nm and 200 nm pores [5] have shown some influence from surface-induced nucleation effects whereas the complete suppression of heterogeneous nucleation was found in smaller pores. Surface-enhanced crystallization kinetics were also seen in the case of poly(L-lactic acid) within the same AAO although the pertinent mechanism of nucleation (heterogeneous/homogeneous) was not discussed [39]. To explore this effect in more detail we examined the roughness of the internal pore surface with AFM. Fig. 8a shows a 3D view of an AFM image of the exposed cross section of the AAO sample. The latter was used to identify a region where the inner wall of a pore was exposed. Subsequently, images of such inner pore wall regions were recorded. To determine the root-mean-square (RMS) roughness of the pore walls, a polynomial surface of 3rd order was subtracted from the height image data, to correct for tilt and average curvature of the sample region. Then a square region of 50 nm × 50 nm within the pore was selected to calculate the RMS roughness using the Histogram function of the software. The analysis provided a RMS roughness of about 0.6 nm, *i.e.,* the internal AAO pore surface is smooth. This result is consistent with the absence of surface-induced effects on the nucleation process. It shows that AAO internal pore surface cannot be held responsible for the nucleation process, especially within the smaller pores.

4. Conclusions

In this work we explored the role of “intrinsic” and “extrinsic” effects in the heterogeneous nucleation process of poly(ethylene oxide) by applying some stringent tests to the confined crystallization of PEO.

- We found that the nucleation mechanism can be altered by a surface layer on top of the templates. When a surface layer connects the pores, heterogeneous nucleation becomes the dominant nucleation mechanism.
- Oligomers shift the homogeneous nucleation temperature to lower temperatures, reflecting the plasticizing effect of the liquid-to-glass temperature. Chain polydispersity and mixing with melt miscible chains does not alter significantly the nucleation process. In both cases, homogeneous nucleation of the majority component remains unaltered.
- The internal pore surface roughness is very small and this explains the minor effects of surfaces on inducing heterogeneous nucleation, especially within the smaller pores.

The results presented here further strengthen the view that heterogeneous nucleation is caused by “objects” that are “extrinsic” to the polymer; these are *impurities* different from polydisperse chains, oligomers, mixtures, etc. Their origin can be traced back to the synthetic methods, like the use of catalyst, salts, etc. Along these lines, the very large spherulites of PEO can be understood by the absence of a metal catalyst. Work in this direction and as a function of polymer architecture is currently in progress.

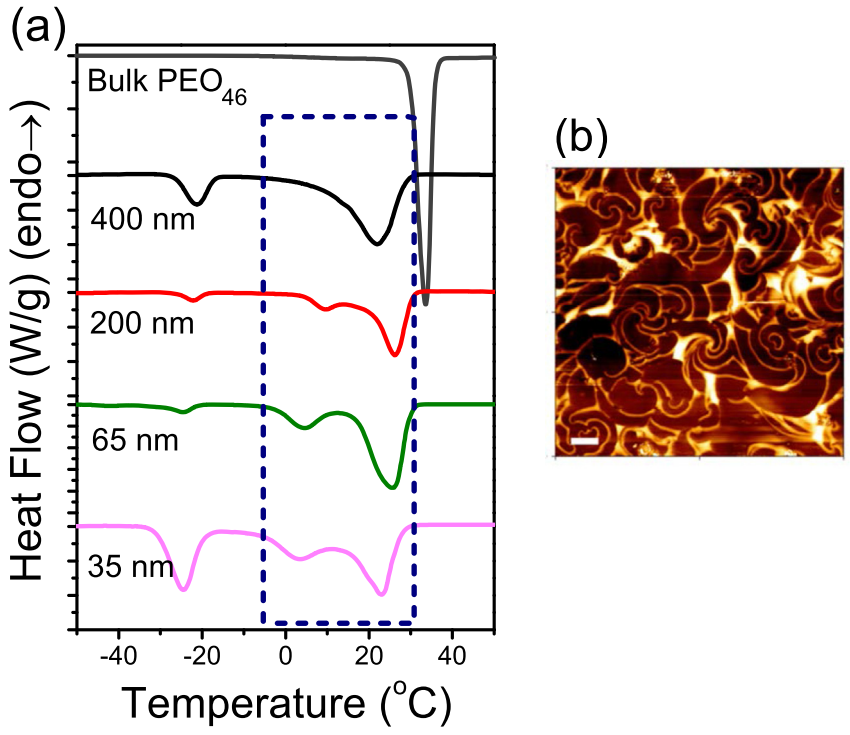

Fig. 7. (a) Cooling thermograms of bulk PEO_{46} and of PEO_{46} located inside AAO with pore diameters ranging from 400 nm to 35 nm in the presence of a top (*i.e.*, connecting) layer. The dashed rectangle indicates the temperature range of heterogeneous nucleation. (b) AFM phase image of PEO_{46} with a layer on top of an AAO template. The white scale bar corresponds to 1 μm. The color scale in the image describes from 0° of black to 35° of white. (For interpretation of the references to colour in this figure legend, the reader is referred to the web version of this article.)

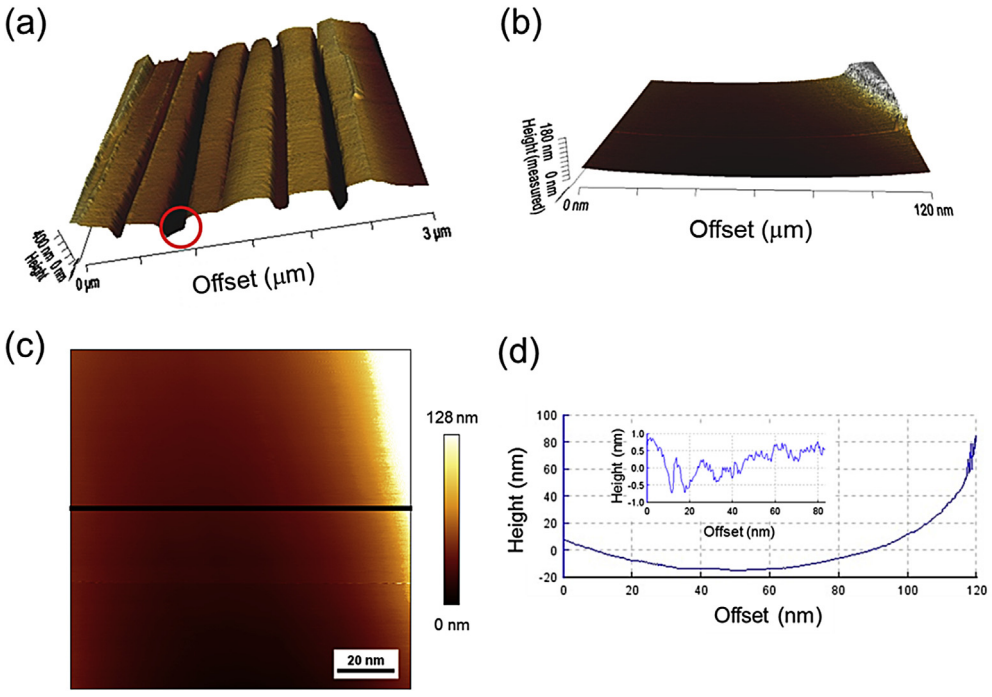

Fig. 8. (**a**) 3D AFM image of AAO with pore diameters of 200 nm. AAO template was vertically cut with metal cutter and cross sectional image was measured. (**b**) Magnified 3D AFM image at near the edge of the pore wall. (**c**) 2D AFM image of the same data as in (b). (**d**) Height profile taken from (c) at the location indicated by the black line. Inserted graph corresponds to the roughness profile inside the pore that was obtained after subtracting a polynomial fit with order of 3 from the original image to separate roughness and average curvature of the pore wall.

Acknowledgements

The current work was supported by the operational program of the NSRF "Aristeia" co-financed by the European Union and the Greek state. AAO template preparation by C. Hess and H. Tobergte are gratefully acknowledged.

References

[1] M. Alcoutlabi, C.B. McKenna, J. Phys.:Condens. Matter 17 (2005) R461.
[2] M.P. Howard, S.A. Milner, Macromolecules 46 (2013) 6593.
[3] K. Binder, J. Horbach, R. Vink, A. de Virgiliis, Soft Matter 4 (2008) 1555.
[4] H. Duran, M. Steinhart, H.-J. Butt, G. Floudas, Nano Lett. 11 (2011) 1671–1675.
[5] Y. Suzuki, H. Duran, W. Akram, M. Steinhart, G. Floudas, H.-J. Butt, Soft Matter 9 (2013) 9189–9198.
[6] Y. Suzuki, H. Duran, M. Steinhart, H.-J. Butt, G. Floudas, Macromolecules 47 (2014) 1793–1800.
[7] Y. Suzuki, H. Duran, M. Steinhart, H.-J. Butt, G. Floudas, Soft Matter 9 (2013) 2621–2628.
[8] M.V. Massa, K. Dalnoki-Veress, Phys. Rev. Lett. 92 (2004) 255509.
[9] Y.-L. Loo, R.A. Register, A.J. Ryan, Phys. Rev. Lett. 84 (2000) 4120.
[10] G. Reiter, G. Castelein, J.-U. Sommer, A. Röttele, T. Thurn-Albrecht, Phys. Rev. Lett. 87 (2001) 226101.
[11] E. Woo, J. Huh, Y.G. Jeong, K. Shin, Phys. Rev. Lett. 98 (2007) 136103.
[12] M. Steinhart, P. Göring, H. Dernaika, M. Prabhukaran, U. Gösele, E. Hempel, T. Thurn-Albrecht, Phys. Rev. Lett. 97 (2006) 027801.
[13] R.M. Michell, A.T. Lorentzo, A.J. Müller, M.-C. Lin, H.-L. Chen, I. Blaszczyk-Lezak, J. Martin, C. Mijangos, Macromolecules 45 (2012) 1517–1528.
[14] R.M. Michell, I. Blaszczyk-Lezak, C. Mijangos, A.J. Müller, Polymer 54 (2013) 4059.
[15] J. Martin, A. Nogales, C. Mijangos, Macromolecules 46 (2013) 7415.
[16] M.M. Elmahdy, K. Chrissopoulou, A. Afratis, G. Floudas, S.H. Anastasiadis, Macromolecules 39 (2006) 5170.
[17] Y. Guan, G. Liu, P. Gao, L. Li, G. Ding, D. Wang, ACS Macro Lett. 2 (2013) 181–184.
[18] Y. Suzuki, H. Duran, M. Steinhart, M. Kappl, H.-J. Butt, G. Floudas, Nano Lett. 15 (2015) 1987–1992.
[19] Y. Suzuki, M. Steinhart, H.-J. Butt, G. Floudas, J. Phys. Chem. B 119 (2015) 11960–11966.
[20] Y. Suzuki, M. Steinhart, R. Graf, H.-J. Butt, G. Floudas, J. Phys. Chem. B 119 (2015) 14814–14820.
[21] H. Masuda, K. Fukuda, Science 268 (1995) 1466.
[22] H. Masuda, F. Hasegawa, S.J. Ono, Electrochem. Soc. 144 (1997) L127.
[23] H. Masuda, K. Yada, A. Osaka, Jpn. J. Appl. Phys. 37 (1998) L1340.
[24] M. Steinhart, Adv. Polym. Sci. 220 (2008) 123.
[25] R. Androsch, A.M. Rhoades, I. Stolte, C. Schick, Eur. Polym. J. 66 (2015) 180.
[26] E. Zhuravlev, J.W.P. Schmelzer, B. Wunderlich, C. Schick, Polymer 52 (2011) 1983.
[27] A. Wurm, E. Zhuravlev, K. Eckstein, D. Jehnichen, D. Pospiech, R. Androsch, B. Wunderlich, C. Schick, Macromolecules 45 (2012) 3816.
[28] H. Duran, A. Gitsas, G. Floudas, M. Mondeshki, M. Steinhart, W. Knoll, Macromolecules 42 (2009) 2881.
[29] F. Kremer, A. Schoenhals, Broadband Dielectric Spectroscopy, Springer, Berlin, 2002.
[30] G. Floudas, Dielectric spectroscopy, in: K. Matyjaszewski, M. Möller (Eds.), Polymer Science: a Comprehensive Reference, vol. 2.32, Elsevier BV, Amsterdam, 2012, pp. 825–845.
[31] G. Floudas, M. Paluch, A. Grzybowski, K.L. Ngai, Molecular Dynamics of Glass-Forming Systems. Effects of Pressure Springer, 2011.
[32] S. Havriliak, S. Negami, Polymer 8 (1967) 161.
[33] V. Harmandaris, K. Kremer, G. Floudas, Phys. Rev. Lett. 110 (2013) 165701.
[34] G. Floudas, W. Steffen, E.W. Fischer, W. Brown, J. Chem. Phys. 99 (1993) 695–703.
[35] A. Deres, G.A. Floudas, K. Müllen, M. Van der Auweraer, F. De Schryver, J. Enderlein, H. Uji-i, J. Hofkens, Macromolecules 44 (2011) 9703.
[36] L.J. Fetters, D.J. Lohse, D. Richter, T.A. Witten, A. Zirkel, Macromolecules 27 (1944) 4639.
[37] G. Floudas, G. Reiter, O. Lambert, P. Dumas, Macromolecules 31 (1998) 7279–7290.
[38] M. Steinhart, S. Senz, R.B. Wehrspohn, U. Gösele, J.H. Wendorff, Macromolecules 36 (2003) 3646.
[39] Y. Guan, G. Liu, G. Ding, T. Yang, A.J. Müller, D. Wang, Macromolecules 48 (2015) 2526–2533.